- **Transport Processes in Neutron Stars: The need for better microphysics inputs for X-ray Burst and Superburst Modeling**

Sanjib S. Gupta (T-16,LANL)
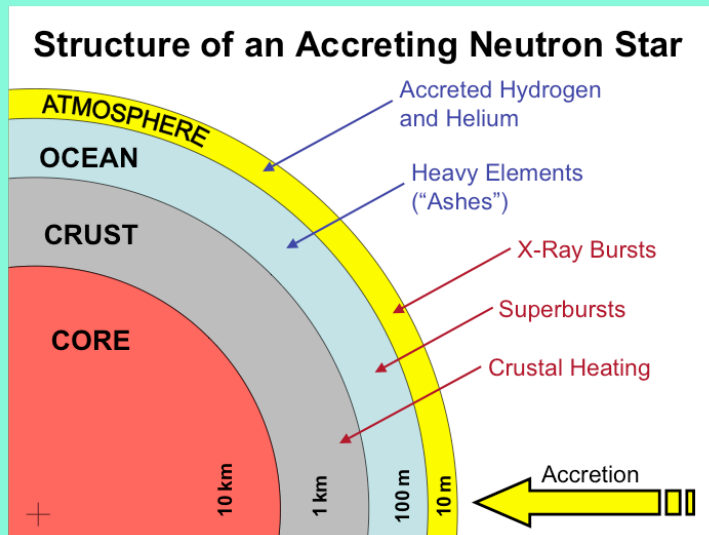
LANL Collaborators:

Alexander Heger (T-6)

Peter Moller (T-16)

Jerome Daligault (T-15)

Sanjay Reddy (T-16)

H/He burning on the surface of Accreting NS

Structure of an Accreting Neutron Star

ATMOSPHERE

OCEAN

CRUST

CORE

Accreted Hydrogen and Helium

Heavy Elements ("Ashes")

X-Ray Bursts

Superbursts

Crustal Heating

10 km   1 km   100 m   10 m

Accretion

* In a LMXB system, the more massive star with shorter lifetime can leave behind a Neutron Star (NS) after core-collapse, which can accrete H/He-rich material from the low-mass companion through a disk.

*Degenerate conditions at the base of the accreted atmosphere can lead to a thermal instability if the heat lost by radiation transport (photons and free-streaming neutrinos) cannot cope with the (local) nuclear energy production.

*Hydrogen burning is ignited through the "hot-CNO" cycle, with breakout reactions such as $^{15}O(\alpha, \gamma)^{19}Ne$ at around $4 \cdot 10^8$ K . The hot-CNO-cycle is $^{12}C(p, \gamma)^{13}N(p, \gamma)^{14}O(\beta^+)^{14}N(p, \gamma)^{15}O(\beta^+)^{15}N(p, \alpha)^{12}C$, a catalytic conversion of 4^1H into ^4He

*Movement from the CNO cycles towards Fe-group nuclei is strongly temperature dependent. At low temperature a slow "rp-process" begins with 2p-captures on an even-even nucleus, a β^+ decay, p-capture, a β^+ decay, and a final (p, α) reaction close to stability on odd-Z targets such as ^{15}N, ^{19}F, ^{23}Na, ^{27}Al, ^{31}P, ^{35}Cl: these are the nuclei at which the H-burning cycles are connected resulting in the CNO-,NeNa-,MgAl-,SiP-,SiCl-cycles. The flow to heavier elements is determined by the $(p,\gamma)/(p, \alpha)$ rate ratio into the next cycle. Burning timescales are therefore sensitive to an accurate determination of these ratios. At around $3 \cdot 10^8$ K all the sub-cycles are open except the CNO-, which awaits the $^{15}O(\alpha, \gamma)^{19}Ne$ reaction.

*Breakouts from these sub-cycles can occur at higher temperatures via p- or α-capture on an unstable isotope in the cycle, such as the $^{15}O(\alpha, \gamma)$, $^{23}Mg(p, \gamma)$, $^{27}Si(p, \gamma)$,$^{31}S(p, \gamma)$ reactions, which limit storage times in the sub-cycles. *However, if these timescales become comparable to or exceed the macroscopic timescales then the cycle is the endpoint of the rp-process and the steady-flow abundance in the sub-cycle determines the final nucleosynthesis abundance distribution.*

*Higher temperatures from thermal feedback shift the process closer to the proton drip line (higher Coulomb barriers can be overcome) with high (p, γ) reaction rates and the *slowest reactions in the sub-cycles become the* β^+ *decays which act as "Waiting Points"* . The rp-process is now significantly **impeded by (γ,p) photo-disintegrations** and the proton capture process may stop altogether leading to decreasing thermal feedback and a "freezout" - i.e. if the (p, γ) rates fall below the β^+ decay rates on a nucleus it becomes substantially enriched in the freezout abundance profile - *the "ashes of the rp-process"*

H/He burning -Part II

A further complication at high temperatures and densities, is the competition of the so-called "αp-process" when temperatures are high enough to overcome the alpha-particle Coulomb barrier. This usually populates excited states above proton thresholds so that the reaction sequence is (α,p) (p,γ). This bypassing of β-decays between even-even nuclear network nodes is seen starting at Oxygen isotopes around $4 \cdot 10^8$K upto Ar.

He burns by the 3α-reaction into ^{12}C. Apart from the thermal feedback between the H and He layers (which enhance reaction rates) there are also chemical feedback effects which can be amplified by Rayleigh-Taylor unstable "plumes" which we can model in 3D mixing. The proton captures ^{12}C(p, γ)^{13}N(p, γ)^{14}O are very fast, so the 3α-process enhances hot-CNO burning, whose rate depends on the mass fraction of CNO isotopes. At the same time the ^{15}N(p, α)^{12}C reaction increases the He concentration and feeds the 3α ! Ignition in a mixed H/He burst comes from unchecked thermal feedback from the 3α-process when the EOS (which determines Pressure response and consequent entropy generation to temperature/density perturbations) is set by the degenerate electron Fermi gas (the stellar environment does not "immediately" expand and cool as in non-degenerate quiescent burning).

Depending on the thermal conditions, the hot-CNO breakout can return to ^{15}O via the hot-CNO-bicycle pathway ^{19}Ne(β$^+$)^{19}F(p, α)^{16}O (p, γ)^{17}F (p, α)^{18}Ne (β$^+$)^{18}F(p, α)^{15}O and accelerate conversion of Hydrogen to Helium , thus affecting the runaway.
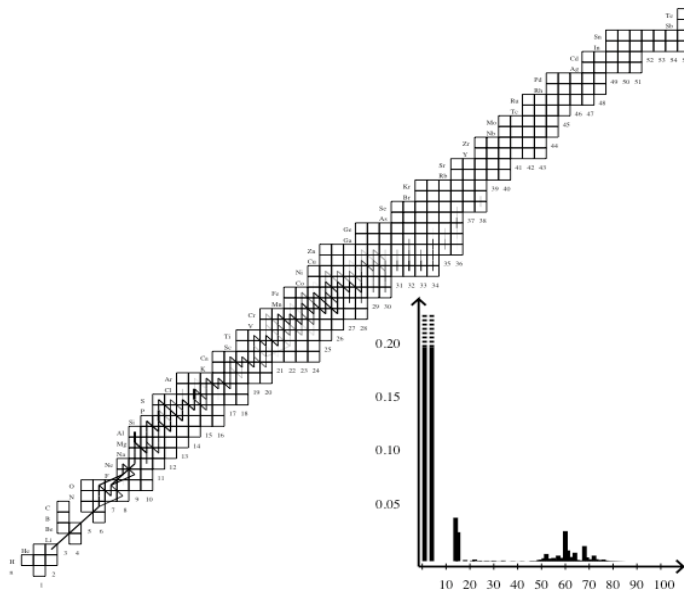

Fig. 13.— Above ignition: $T = 4.44 \cdot 10^8$K, $\rho = 3.46 \cdot 10^5$g/cm^3, $X = 0.398$, $Y = 0.402$, $t = -11.091$s. (see end of §4 for an explanation of the diagram).

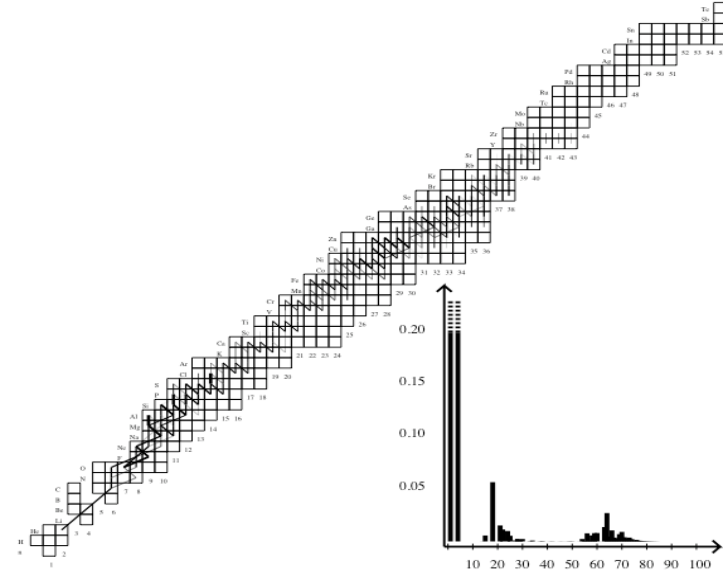Fig. 15.— Above ignition: $T = 6.97 \cdot 10^8$K, $\rho = 2.51 \cdot 10^5$g/cm^3, $X = 0.381$, $Y = 0.372$, $t = -9.994$s. (see end of §4 for an explanation of the diagram).

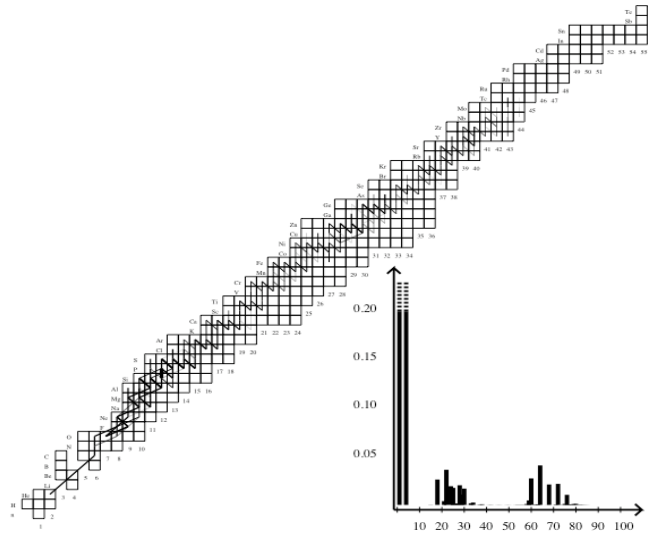Fig. 16.— Above ignition: $T = 8.34 \cdot 10^8$K, $\rho = 2.15 \cdot 10^5$g/cm³, $X = 0.358$, $Y = 0.346$, $t = -9.097$s. (see end of §4 for an explanation of the diagram).
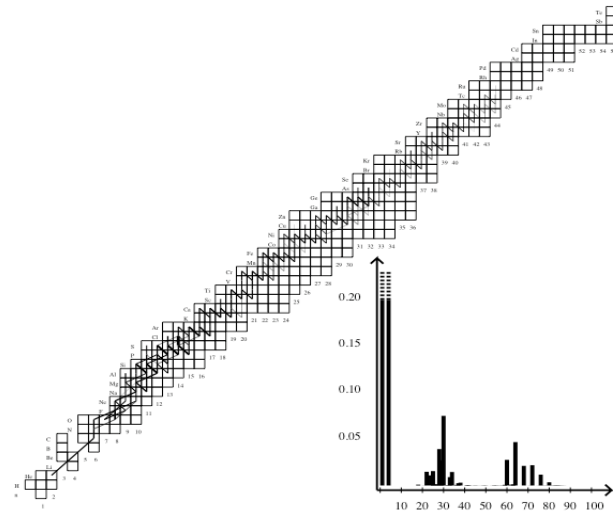
Fig. 17.— Above ignition: $T = 8.96 \cdot 10^8$K, $\rho = 2.07 \cdot 10^5$g/cm³, $X = 0.327$, $Y = 0.326$, $t = -8.075$s. (see end of §4 for an explanation of the diagram).
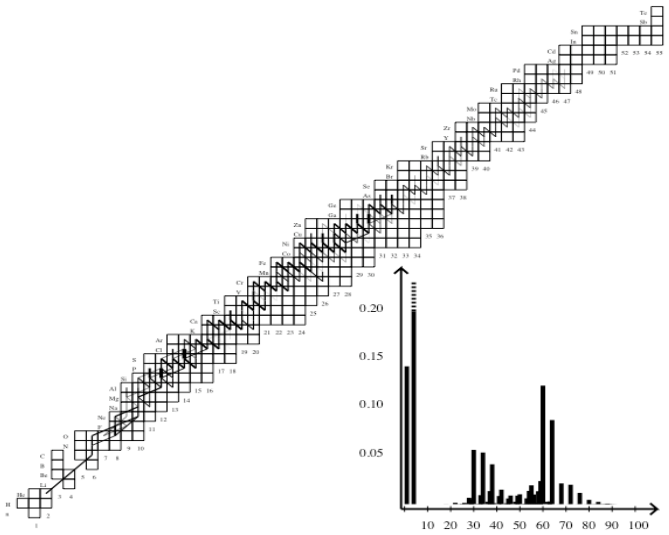
Fig. 18.— Above ignition: $T = 9.93 \cdot 10^8$K, $\rho = 2.43 \cdot 10^5$g/cm³, $X = 0.143$, $Y = 0.234$, $t = -3.013$s. (see end of §4 for an explanation of the diagram).
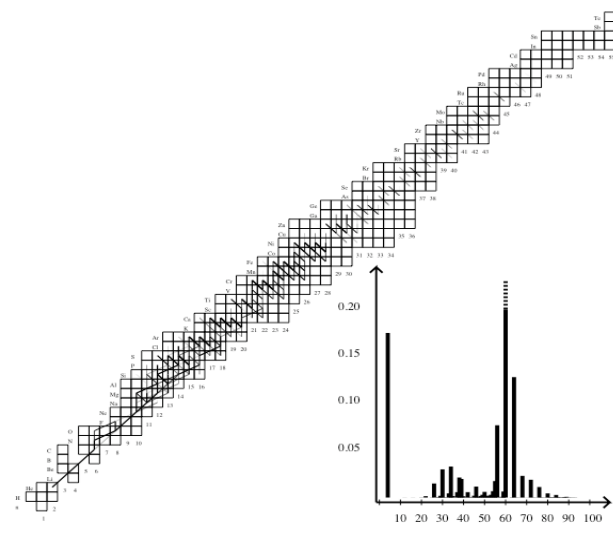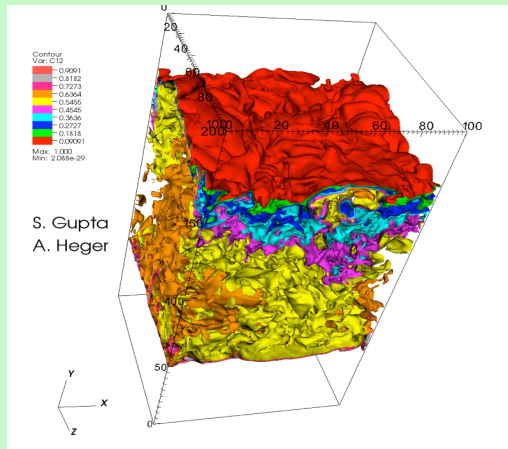
Fig. 19.— Above ignition: $T = 9.62 \cdot 10^8$K, $\rho = 3.54 \cdot 10^5$g/cm³, $X = 2.5 \times 10^{-5}$, $Y = 0.175$, $X_{60} = 0.346$, $t = 1.476$s. (see end of §4 for an explanation of the diagram).

Evolutionary snapshots of accreted parcel of matter from Fisker et.al. astro-ph/070331 with t=0 at peak surface luminosity.

3D hydrodynamical models of the XRB:Crust Composition Dependencies

From 1-D multi-zone models of XRB evolution we take compositional and thermodynamic profiles to study the interaction of the H and He convective layers.

The timescale for mixing and burning of H determines how close to the surface the convection penetrates. This affects the rise time of the light curve.

The tail of the light curve depends on how the ^{12}C from the helium layer interacts with the Hydrogen layer - if only a little mixes then the slower rp-process which stalls at the proton drip-line dominates - and upto A=100 elements are produced. This will correspond to an observational signature of slow rise and decay of the lightcurve.
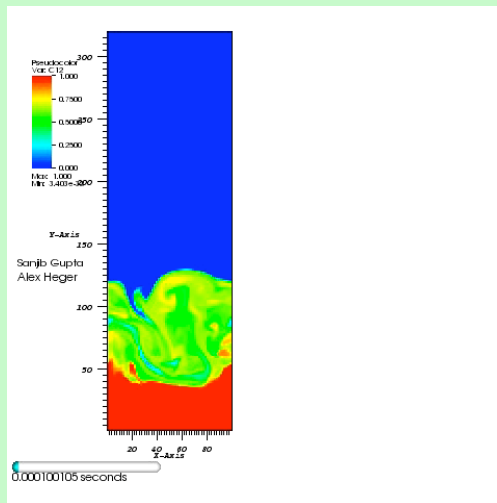
However if most of the ^{12}C mixes then the faster αp-process (also results in a steeper/ faster rise to peak luminosity) bypasses the β-decay Waiting Points resulting in pre-Fe-group light elements with short lifetimes that show up as a steep drop-off in the lightcurve when radioactive species are exhausted.

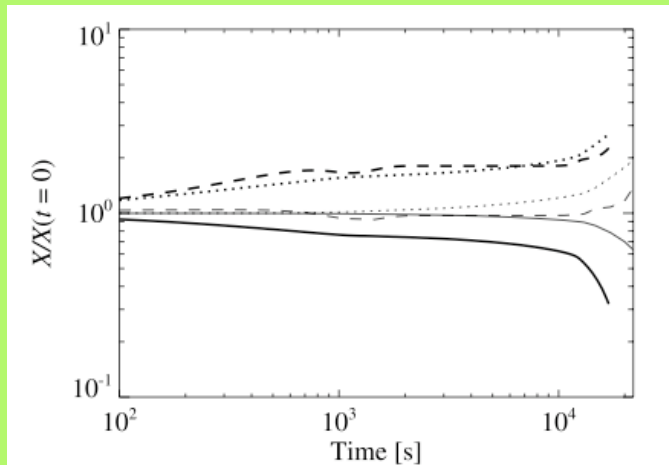# *Separation of CNO isotopes from H- Diffusion in MCP*

FIG. 2.—Evolution of mass fractions of H (*solid lines*), He (*dotted lines*), and CNO elements (*dashed lines*), normalized to their initial values as a function of Lagrangian time $t = y/\dot{m}$ for $\dot{m} = 0.11\dot{m}_{Edd}$. We show cases when diffusion is (*thick lines*) and is not (*thin lines*) included. The curves terminate when He ignites unstably.

FIG. 13.—Ashes produced by the one-zone burst calculation following unstable He ignition for $\dot{m} = 0.11\dot{m}_{Edd}$. The initial composition is taken from the bottom of the fuel layer at the point at which ^{4}He ignites, for the calculation with (*circles and solid lines*) and without (*plus signs and dotted lines*) sedimentation and diffusion.

A major complication in calculating timescales of nuclear burning is that an ionized stellar plasma in a gravitational field does not move as a composite XRB "ash" parcel : lighter ions float upwards through the ashes and an electric field is generated by the composition gradients that are established (after self-consistently solving for charge neutrality and Hydrostatic Equilibrium).

There is a very large range of plasma conditions under which we need to model this non-equilibrium plasma (inter-) diffusive process: from $\Gamma<1$ ranging to beyond 173, which would correspond to crystallization in the OCP.

Peng et.al. 2007 (ApJ 654:1022-1035, from which figures on left are shown) showed that even for high accretion rates ~0.1m_{edd} the H abundance at the base of the accreted layer is significantly reduced, due to the diffusive separation. Since the timescale for the plasma diffusive separation is of the order of the accretion timescale (time to replenish the accreted column to where is becomes thermally unstable to nuclear reactions), we are missing a crucial piece of the puzzle of H/He/CNO burnings ! The accretion rate at which mixed H/He ignition occurs changes by a factor of 2 simply by coupling the diffusive separation to the nuclear burning evolution.

Finally, a crucial missing ingredient in Superburst ignition is getting enough ^{12}C to survive at 10^9 g cm^{-3} : Sedimentation can substantially change the destruction of ^{12}C by hydrogen burning since it lowers the proton-to-capture-seed ratio in the rp-process and decreases the mean mass of the end composition.

This underscores why we are so interested in sedimentation - the separative process changes **the concentration of nuclear reactants at a depth**, and changes the nuclear burning profile ! Thus the observed energetics could change completely depending on the transport coefficients in our model !

Further, Electron Captures in the Crust make matter increasingly neutron-rich, increasing their susceptibility to gravitational settling vs. the electric field acting on them. The effects will be much stronger than on ^{22}Ne - thus crust nucleosynthesis as we know it could be very different, and further impact the energetics of the crust.
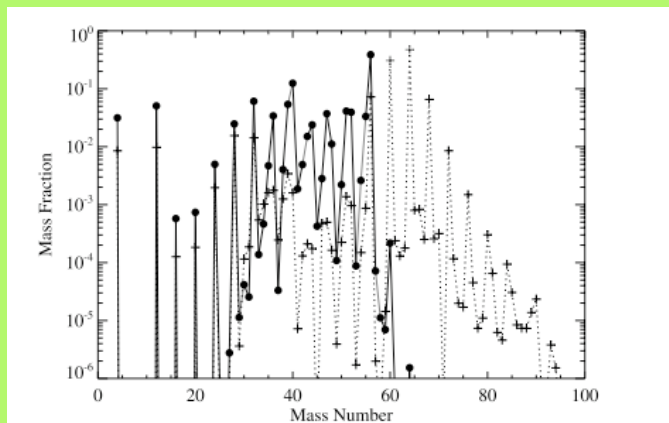
The pure one component plasma (OCP) phase diagram is well known. The liquid solidifies when the ratio of a typical Coulomb energy to the thermal energy kT is $\Gamma \approx 175$ [11]. The parameter Γ is defined,

$$\Gamma = \frac{Z^2 e^2}{aT},\qquad(1)$$

where the ion charge is Ze, the temperature is T, and the ion sphere radius a describes a typical distance between ions, $a = (3/4\pi n)^{1/3}$. Here n is the ion (number) density.

Plasma conditions over the atmosphere and crust of NS range from $\Gamma \ll 1$ to beyond $\Gamma \sim 200$. However, the current astrophysical models assume $\Gamma \ll 1$ and describe diffusion as independent binary collisions between Debye-screened particles . This will break down over the range of Γ we are interested in and miss effects such as rapid oscillations in a transient cage formed by nearest neighbors - liquidlike behavior for $\Gamma \sim 10$ (Donko et.al. Phys.Plasmas 10, 1563 (2003)).

The only other approximations in use are classical OCP self-diffusion coefficients for a single representative species (Bildsten and Hall, ApJ 549:L219 which uses the fit of Hansen et.al. Phys.Rev.A 11, 1025(1975)) . This simple power-law fit is extensively discussed in Daligault and Murillo Phys.Rev.E 71, 036408 (2005) and shown to be accurate to only 20% or so to actual MD simulations

$$D = \omega_p a^2 \frac{2.95}{\Gamma^{1.34}},$$

where $\omega_p = \sqrt{4\pi(Ze)^2 n/M}$ is the ion plasma frequency

as crystallization approaches, collective effects play an increasingly important role and diffusion is dominated by many body physics ! We must cover the entire regime of temperature and density conditions that comprise the Neutron Star interior to understand the timescales of non-equilibrium processes.

Coupled Mechanical, Thermal and Nuclear Evolutionary models of the Crust - setting the thermal profile !

* Hydrostatic Equilibrium under GR conditions - Tolman-Oppenheimer-Volkoff equation gives condition for pressure balancing the gravitational force

$$\frac{\partial r}{\partial a} = (4\pi r^2 n)^{-1}\left(1 - \frac{2Gm}{rc^2}\right)^{\frac{1}{2}}$$

$$\frac{\partial m}{\partial a} = \frac{\rho}{n}\left(1 - \frac{2Gm}{rc^2}\right)^{1/2}$$

$$\frac{\partial \Phi}{\partial a} = \frac{Gm}{4\pi r^4 n}\left(1 + \frac{4\pi r^3 P}{mc^2}\right)\left(1 - \frac{2Gm}{rc^2}\right)^{-1/2}$$

$$\frac{\partial P}{\partial a} = -\frac{Gm\rho}{4\pi r^4 n}\left(1 + \frac{P}{\rho c^2}\right)\left(1 + \frac{4\pi r^3 P}{mc^2}\right)\left(1 - \frac{2Gm}{rc^2}\right)^{-1/2}$$

where a = the total number of baryons inside sphere of radius "r" and

- ρ = Mass Density, the potential Φ appears in time-time component of the Schwarzschild metric as e^{Φ/c^2} and governs the redshift of photons and neutrinos. At the stellar surface

$$e^{2\Phi/c^2}\big|_{r=R} = 1 - \frac{2GM}{Rc^2}$$

- Where M=total gravitational mass and $4\pi R^2$ = surface area of the neutron star. Here n = baryon density and m=mass within radius =r

- P(n) is obtained from the EOS by summing the electron, ion and neutron energy density contributions in the outer crust by following the BPS method – electrons are a highly degenerate relativistic Fermi gas,

- Crust EOS is determined pre-ND ($< 4 \bullet 10^{11}$ g/cc) using BPS prescription : sum electron (get pressure from Helmholtz Free Energy Tabulation-partial derivatives) + ionic + lattice (fits) + free neutrons. Compressible liquid-drop model allows for an external neutron gas.

- Free neutrons are present for $n > 3.6 \bullet 10^{-4} \, fm^{-3}$ and dominate the pressure when $n > 0.04 \, fm^{-3}$ in which regime the P(n) fit of Negele and Vautherin is used. (Negele & Vautherin, 1973, Nucl.Phys.A,207,298)

- At $n > 0.1 \, fm^{-3}$ nuclei dissolve into uniform nuclear matter and we use Akmal et.al. 1998 AV18+dv+UIX results using the Argonne V18 potential with relativistic boost corrections and the TNI =UIX. Neutrons, protons, electrons and where Electron Fermi Energy > rest mass of muon = 105.66 MeV, muons contribute. (Akmal et.al. 1998, Phys. Rev. C vol.58 #3)

- Hyperons/quark matter are not contributors to our EOS.

- For each baryon density we obtain the proton fraction and electron fraction from beta-equilibrium and charge neutrality

$$Y_p = n_p / n$$
$$Y_e = n_e / n$$
$$\mu_n - \mu_p = \mu_e = \mu_\mu$$
$$n_p = n_e + n_\mu$$
$$\rho = nH(n, Y_p, Y_e, Y_\mu) / c^2 = \varepsilon / c^2$$
$$P = n^2 \frac{\partial H}{\partial n} = c^2 \left(-\rho + n \frac{\partial \rho}{\partial n} \right)$$

- P(rho) of AV18+dv+UIX matches Negele and Vautherin at $n = 0.078 \, fm^{-3}; P = 0.039 \, MeVfm^{-3}$ thus facilitating a smooth transition from crust to core without density discontinuity.

- With P(n) specified integrate structure equations out from fixed central pressure to atmospheric density – compute gravitational mass, adjust central pressure to fit target mass, iterate.

- Steady – State Thermal profile is calculated from solving the entropy and flux equations (L=luminosity, T=proper temperature)

$$e^{-2\Phi/c^2} \frac{\partial}{\partial r}\left(Le^{2\Phi/c^2}\right) - 4\pi r^2 n\left(\varepsilon_N - \varepsilon_\upsilon\right)\left(1 - \frac{2Gm}{rc^2}\right)^{-1/2} = 0$$

$$e^{-\Phi/c^2} K \frac{\partial}{\partial r}\left(Te^{\Phi/c^2}\right) + \frac{L}{4\pi r^2}\left(1 - \frac{2Gm}{rc^2}\right)^{-1/2} = 0$$

- Where ε_N = nuclear heating from EC and neutron reactions and ε_υ =

crust/core neutrino processes. K=conductivity calculated from composition.

Boundary Conditions on Luminosity are set by flux at r = R (obtained from photospheric calculation, temperature at base of H/He burning shell sets the flux as function of accretion rate) and zero flux at r = 0. Additionally the Luminosity at the crust/core interface must match the core neutrino emissivity.

Electron Transport In Dense Coulomb Plasmas - composition-dependent Conductivities under electron-ion scattering

$$\Gamma(\mathbf{p} \to \mathbf{p}') = \frac{2\pi N}{\hbar^2}\frac{1}{2}\sum_{\sigma\sigma'}|U_{\mathbf{q},\sigma'\sigma}|^2\, \mathcal{S}(\mathbf{q},\omega), \qquad (1)$$

$$\mathcal{S}(\mathbf{q},\omega) = \frac{1}{2\pi}\int_{-\infty}^{+\infty} dt\, e^{-i\omega t}\mathcal{S}(\mathbf{q},t)$$

$$= \frac{1}{2\pi N}\int_{-\infty}^{+\infty} dt \int d\mathbf{x}\, d\mathbf{x}'\, e^{i\mathbf{q}\cdot(\mathbf{x}-\mathbf{x}')-i\omega t}$$

$$\times \langle \hat{\rho}^\dagger(\mathbf{x},t)\,\hat{\rho}(\mathbf{x}',0)\rangle_T, \qquad (2)$$

where N is the total number of ions, $\mathbf{p}$ and $\mathbf{p}'$ are the electron momenta before and after scattering, respectively, $\hbar\mathbf{q} = \mathbf{p}' - \mathbf{p}$, $\hbar\omega = \epsilon' - \epsilon$ is the difference between final and initial electron energies, and $U_{\mathbf{q},\sigma'\sigma}$ is the matrix element of the operator of elementary ei interaction. $\mathcal{S}(\mathbf{q},\omega)$ is the dynamical structure factor of the plasma, the most important quantity of the theory. In the liquid regime, $\hat{\rho}(\mathbf{x},t)$ is the operator of the charge density in units of $Z|e|$: $\hat{\rho}(\mathbf{x},t) = \hat{n}_I(\mathbf{x},t) - n_i$, where $\hat{n}_I(\mathbf{x},t)$ is the ion density operator and $n_i = n_e/Z$ takes account of the compensating electron background with the electron density n_e. In the solid regime, $\hat{\rho}(\mathbf{x},t) = \hat{n}_I(\mathbf{x},t) - \sum_i \delta(\mathbf{x}-\mathbf{R}_i)$ (where $\mathbf{R}_i$ is a lattice vector), i.e. the operator of fluctuations of the charge density.

SCCP of ions in a uniform electron gas (charge compensating) - disordered or in a crystal lattice.

Differential scattering electron-ion rate averaged over initial and summed over final electron spin states on left (from Baiko et.al. 1998)

$$\sigma = \frac{n_e e^2}{m_e^* \nu_\sigma}, \qquad \kappa = \frac{\pi^2 T n_e}{3 m_e^* \nu_\kappa},$$

where $m_e^* = \epsilon_F/c^2$, and

Effective collision frequency $\nu_{\sigma,\kappa} \sim m_e^*\, Z^2\, e^4\, L\, n_i\,/(k_F^3)$ which sums the differential scattering weighted by statistical phase-space factors over the electron wavevector range to the Fermi Surface

Primary scattering process is electron-impurity (**but need composition dependence**!) not e-p or e-e: so Itoh and Kohyama (ApJ 404, 268) fits are used to compositionally weight the scattering from single-component scattering….assumes there are no clustering/separation effects!

$$\langle S\rangle = \int_0^1 d\left(\frac{k}{2k_F}\right)\left(\frac{k}{2k_F}\right)^3 \frac{S(k/2k_F)}{[(k/2k_F)^2 \varepsilon(k/2k_F,0)]^2} - \frac{1.018(Z/A)^{2/3}\rho_6^{2/3}}{1+1.018(Z/A)^{2/3}\rho_6^{2/3}}$$

$$\times \int_0^1 d\left(\frac{k}{2k_F}\right)\left(\frac{k}{2k_F}\right)^5 \frac{S(k/2k_F)}{[(k/2k_F)^2 \varepsilon(k/2k_F,0)]^2}$$

where $\hbar k$ is the momentum transferred from the ionic system to an electron, $S(k/2k_F)$ the ionic liquid structure factor, and $\varepsilon(k/2k_F,0)$ the static dielectric screening function due to degenerate electrons. The first term in equation (6) corresponds to the ordinary Coulomb logarithmic term, and the second term is a relativistic correction term.

$$\sigma = 8.693 \times 10^{21}\rho_6\left(\sum_i \frac{X_i}{A_i}\right)$$

$$\times \frac{1}{\{1 + 1.018[\sum_i (Z_i/A_i)X_i]^{2/3}\rho_6^{2/3}\}\langle S\rangle}$$

$$\times \frac{\langle Z\rangle^2}{\langle(\Delta Z)^2\rangle}\, s^{-1}, \qquad (21)$$

$$\kappa = 2.363 \times 10^{17} T_8\, \rho_6\left(\sum_i \frac{X_i}{A_i}\right)$$

$$\times \frac{1}{\{1 + 1.018[\sum_i(Z_i/A_i)X_i]^{2/3}\rho_6^{2/3}\}\langle S\rangle}$$

$$\times \frac{\langle Z\rangle^2}{\langle(\Delta Z)^2\rangle}\, \mathrm{ergs\ cm^{-1}\ s^{-1}\ K^{-1}}, \qquad (22)$$

$$\langle Z\rangle \equiv \sum_i x_i Z_i,$$

$$\langle(\Delta Z)^2\rangle \equiv \sum_i x_i(Z_i - \langle Z\rangle)^2,$$

$$x_i \equiv \frac{n_i}{\sum_j n_j}.$$

11
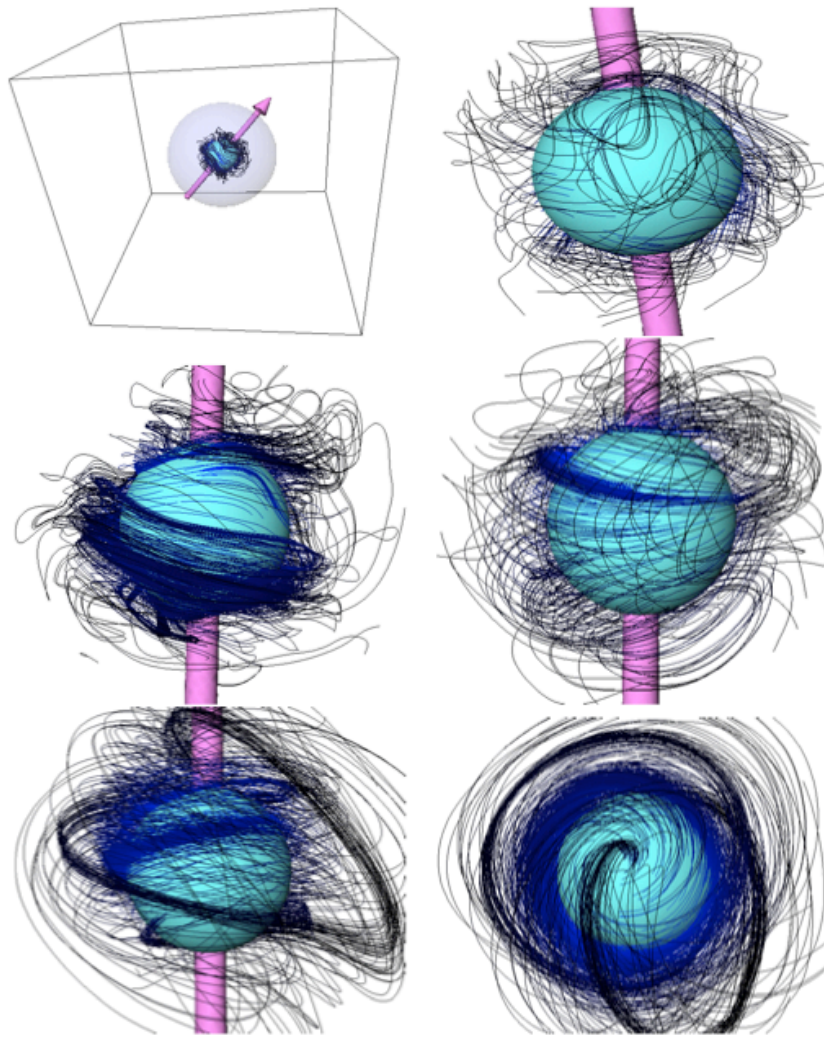
Fig. 6. The initial evolution of the field, plotted with IRIS Explorer. Plotted *top left* at $t = 0$ is the computational box, with field lines, the axis *M* and (only in this frame) the surface of the star. Also plotted in this frame, as in all of the frames, is a surface of constant radius ($r = 0.3\,R_*$), which helps to make it easier to see the field lines in the foreground. However, in this frame this is difficult to see. Therefore, the other frames are zoomed-in somewhat, so that only the $r = 0.3\,R_*$ surface is visible and not the surface of the star. *Top right* is also at $t = 0$, but viewed from a different angle, and zoomed-in. *Middle left, middle right* and *bottom left* are snapshots taken at times $t = 0.18$, 0.54 and 5.4 days. *Bottom right* is the last of these, looking down the magnetic axis.

Braithwaite and Nordlund (A&A 450,1077 (2006)) studied formation of stable **B**-field configurations from initial random configuration on a isentropic stratification in hydrostatic equilibrium.

The stable configuration had a very strong toroidal component….subsequent evolution through magnetic diffusion effects $D \sim \eta c/4\pi$ leads to substantial magnetic energy density in the poloidal component.
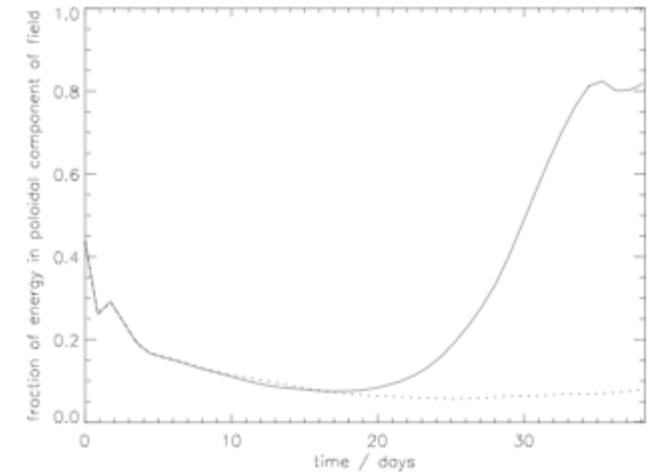
Fig. 7. The fraction of the magnetic energy contained in the poloidal field for the two runs (at resolution 96^3) with the atmospheric diffusion term switched on (solid line) and off (dotted line).

Shape of Magnetic Field affects the Temperature Distribution in the NS Crust through anisotropy in transport (Geppert et.al. A&A 426,267 (2004))

In the relaxation time approximation the components of $\hat{k}$ parallel and perpendicular to the magnetic field, $\kappa_\parallel$ and $\kappa_\perp$ respectively, as well as the Hall component, $\kappa_\wedge$, are related to the scalar heat conductivity κ_0 and to the magnetization parameter $\omega_B\tau$ by (Yakovlev & Kaminker 1994)
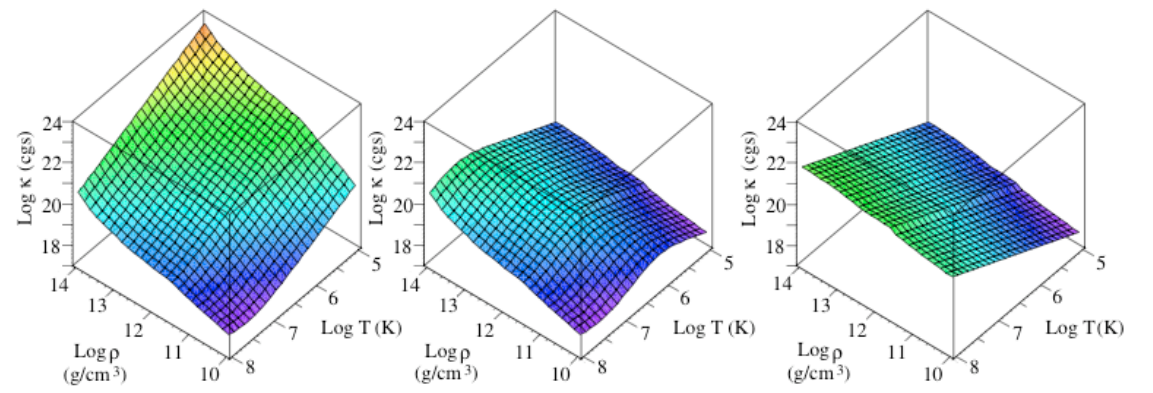
$$\kappa_\parallel = \kappa_0, \quad \kappa_\perp = \frac{\kappa_0}{1+(\omega_B\tau)^2}, \quad \kappa_\wedge = \omega_B\tau\,\kappa_\perp. \qquad (3)$$

For κ_0 we use

$$\kappa_0 = \frac{\pi^2 k_B^2 T n_e}{3 m_* \nu} \qquad (4)$$

where $\nu = 1/\tau$ is the effective electron collisional frequency and is given by the sum

$$\nu = \nu_{\mathrm{ph}} + \nu_{\mathrm{ion}} + \nu_{\mathrm{imp}} \qquad (5)$$

Fig. 1. Thermal conductivity κ_0, in cgs units, versus density ρ and temperature T. The left panel shows the phonon-only contribution $\kappa_{0\,\mathrm{ph}}$, the right one the impurity-only contribution $\kappa_{0\,\mathrm{imp}}$, and the central panel the complete κ_0 (with an impurity concentration $Q_{\mathrm{imp}} = 0.1$).
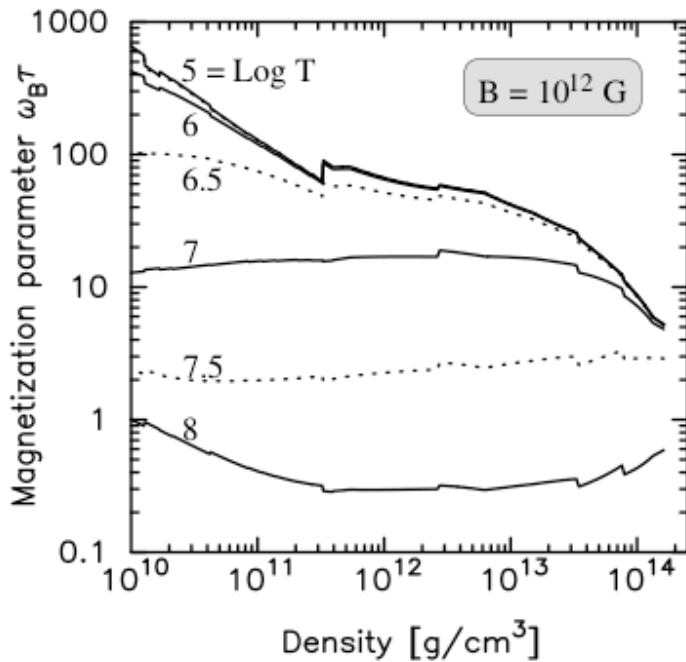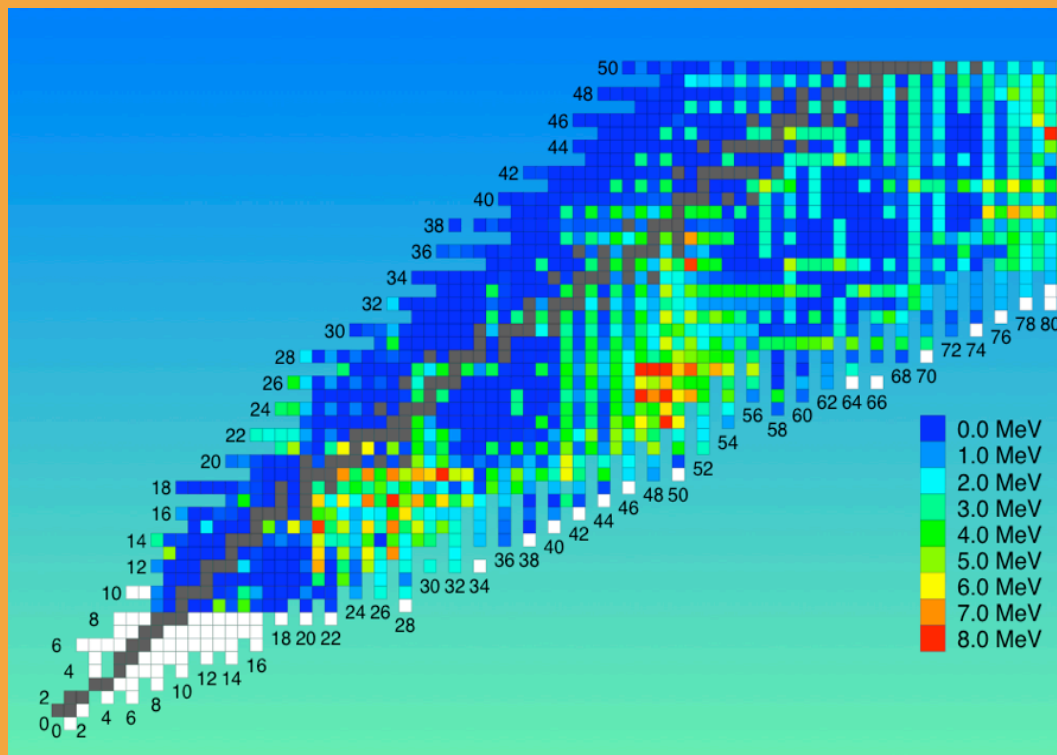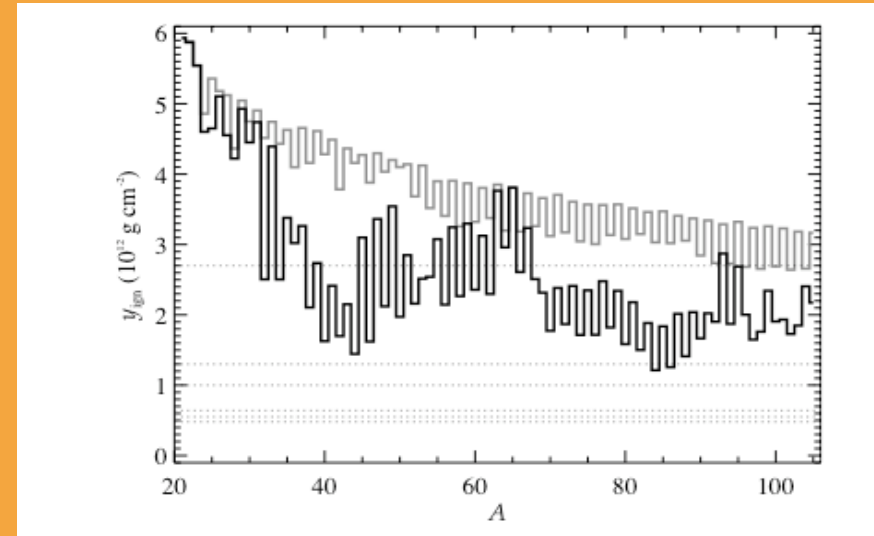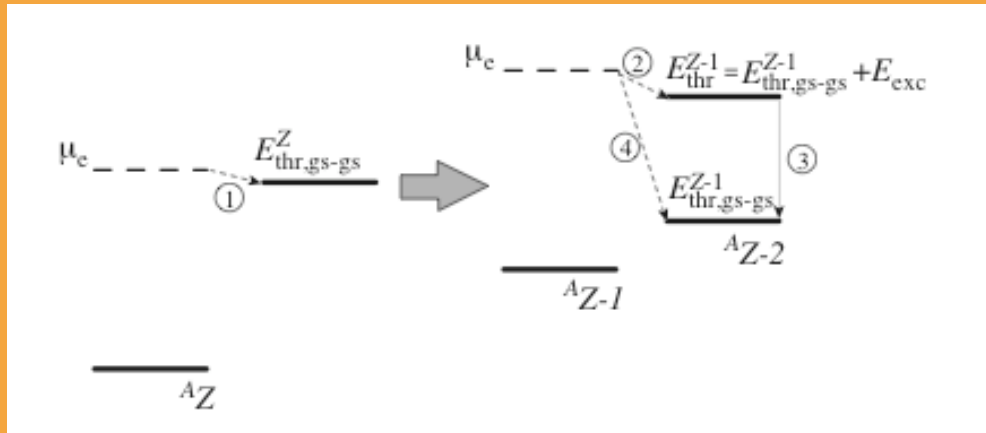

Fig. 2. Magnetization parameter $\omega_B\tau$ vs. density at six different temperatures (as labeled on the curves) assuming a uniform magnetic field of strength $B = 10^{12}$ G. Its value for different field strengths scales linearly in B.
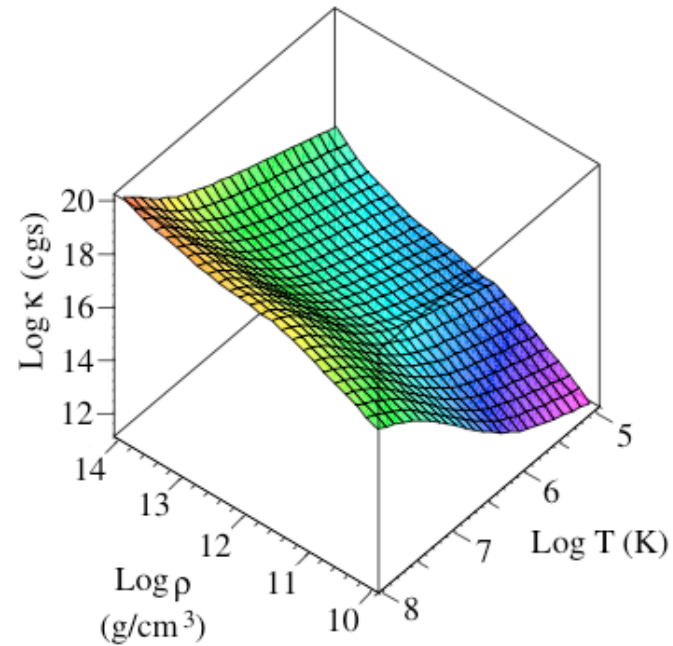
Fig. 3. Thermal conductivity, in cgs units, perpendicular to the magnetic field, $\kappa_\perp$, vs. density ρ and temperature T for a uniform magnetic field of strength 3×10^{12} G. For field strengths $\gg 10^{12}$ G, i.e., for $\omega_B\tau \gg 1$, $\kappa_\perp$ scales as B^{-2}. The impurity parameter Q is assumed to be 0.1.

Deep Crustal Heating Mechanisms and the importance of accurate Nuclear Physics input

Crust Evolution Movie Theatre…..